DOI: http://dx.doi.org/10.32571/ijct.1863360 E-ISSN: 2602-277X

International Journal of Chemistry and Technology

http://dergipark.org.tr/ijct

Research Article

A Robust and Photocatalytic Cr_2O_3@CuO Photocathode for Photoelectrochemical Hydrogen Production

Ender FAKI*[1] Fatih TEZCAN[2] Gökmen SIĞIRCIK[1] Gülfeza KARDAŞ[1]

[1] *Department of Chemical, Faculty of Science and Art , Çukurova University , 01330, Adana, Türkiye.*

[2] *Department of Chemistry and Chemical Process Technology, Vocational School of Technical Sciences at Mersin Tarsus Organized Industrial Zone, Tarsusa University , 33100, Mersin, Türkiye.*

Received: 19 January 2026; Revised: 5 March 2026; Accepted: 16 March 2026

*Corresponding author: *enderfaki@gmail.com*

Citation: Fakı, E., Tezcan, F., Sığırcık, G., & Kardaş, G. (2026). A robust and photocatalytic Cr_2O_3@CuO photocathode for photoelectrochemical hydrogen production. *International Journal of Chemistry and Technology*, 10, 1-7. http://dx.doi.org/10.32571/ijct.1863360

ABSTRACT

The study represents the synthesis of photoelectrodes Cr_2O_3@CuO with hydrothermal and electrochemical deposition (various chronoamperometric deposition of CuO 15, 30 and 45 minutes) for photocathode heterostructure for photoelectrochemical hydrogen production. Cr_2O_3 is more resistant to photocorrosion but performs at a lower photocatalytic performance. Although CuO absorbs in the visible region, it nevertheless enables photocorrosion under mild conditions. According to these advantages of electrodes, Cr_2O_3@CuO photocathode is designed, and Cr_2O_3 photocurrent density increased 9 times to -0.911 mA cm^{-2} (-0.5 V vs. Ag/AgCl) for chronoamperometric deposition of 45 minutes of CuO (S30) under 100 mW cm^{-2} solar irradiance. The surface morphology of Cr_2O_3@CuO photocathode consists of Cr_2O_3 nanosphere and CuO layer, confirmed by scanning electron microscopy. To investigate photostability and catalytic activity on Hydrogen Evolution Reaction (HER) under solar light, electrochemical impedance spectroscopy (EIS) and chronoamperometric measurement are conducted, indicating polarisation resistance (R_p) is dramatically decreased with combined Cr_2O_3@CuO heterostructure compared to pristine Cr_2O_3 electrode, and Cr_2O_3@CuO photocathode performs the most photostability performance (-0.5 V vs. Ag/AgCl) under solar irradiation for 3 hours. Mott-Schottky measurement indicates that Cr_2O_3 and CuO act as p-type semiconductors, and Cr_2O_3@CuO heterostructure conductive band (CB) shifts to a more negative energy level of H^+/H_2 consequently hindering photocorrosion of CuO into the electrochemical double layer.

Keywords: Photocathode, heterojunction, hydrogen evolution reaction, photocorrosion.

1. INTRODUCTION

Hydrogen has become a vital tool for reducing carbon emissions in industries where eliminating fossil-based applications is challenging. Furthermore, the current global energy crisis has emphasised the importance of hydrogen in reinforcing energy security. Several prominent economies have also recently implemented novel industrial strategies in which hydrogen technologies play a critical role (Liu et al., 2023). Green

DOI: http://dx.doi.org/10.32571/ijct.1863360 E-ISSN: 2602-277X

hydrogen production can be performed with water decomposition to O_2 and H_2 products by solar photon energy. The solar-driven water splitting occurs in a photoelectrochemical cell (PEC), including a photoanode and photocathode. Consequently, HER and Oxygen Evolution Reaction (OER) can occur in acidic, mild and basic media over the photocathode (p-type) and photoanode (n-type), respectively. The reactions can only be performed with equal/higher photon energy than the band gap of the semiconductor. The theoretical water splitting potential is about 1.23 V, but it spreads to 1.8-2.0 V due to resistance sources depending on the semiconductor or electrolyte content(Chiu et al., 2019; da Silva Veras et al., 2017; Kayan, 2023.; Tezcan et al., 2023). Therefore, the suggested semiconductor material should absorb solar light in the visible region in terms of the accomplished water splitting with solar irradiance. Moreover, photoelectrodes should become abundant, non-toxic, robust and simple to synthesise according to their counterparts to achieve industrial applications of semiconductors.

The Cr_2O_3 semiconductor serves these benefits; thus, Cr_2O_3 has a preferred variety of studies, such as methanol production (Mahmoud, 2014), solar cells (Khelifa et al., 2019), photoelectrochemical degradation (Zelekew et al., 2021a) and photoelectrochemical cells (Tezcan et al., 2022). However, it is only a limited number of studies in the photoelectrochemical water splitting; lead is worth discovering in this regard. The stable crystal structure of Cr_2O_3 offers the advantage of becoming resistant to photocorrosion and performs absorption in the visible region. Nevertheless, low light absorption coefficients cause low solar light yields of Cr_2O_3. The obstacle of a semiconductor can be eliminated by the contribution of a pair by selecting an appropriate binary semiconductor heterostructure (Mansoor et al., 2023; Zelekew et al., 2021a). Therefore, CuO semiconductor can be suitably nominated over Cr_2O_3 heterostructure regarding cheaper, eco-friendly, high solar light absorption and low E_g energy level for photoelectrochemical water splitting. The heterostructures can be designed as n-p and p-p junctions depending on the selection of the photoelectrode application, such as photoanode and photocathode for photoelectrochemical hydrogen production and photocatalytic systems (Tezcan et al., 2022). For instance, Zelekew et al. studied (Zelekew et al., 2021b) the Cr_2O_3ZnO heterostructure (p-n) photocatalyst for the organic dye degradation by varying the ratio of Cr_2O_3 over Cr_2O_3/ZnO heterostructure, indicating 85% organic dye degradation performance. Mansoor and coworker (Mansoor et al., 2023) fabricated Cr_2O_3/Mn_2O_3 (p-n) binary electrode 1:1 ratio with aerosol-assisted chemical vapour deposition over the FTO at the various calcination temperatures for the OER process. The results indicated a Cr_2O_3/Mn_2O_3 photo-response of 1.25 mA cm^{-2} at 1.23 V (*vs.* NHE), at 500 °C. Also, instead of the photoelectrode heterostructure architecture, such as an n-p and a p-p configuration, catalytic metals (Pt, Ni, Pd, etc.) can be applied over binary heterostructures in the HER process. In a previous study, the Sekizawa group investigated that p-type Cr_2O_3 photocatalytic performance enhanced with n-type TiO_2 and Pt catalytic clusters on photoelectrochemical hydrogen production (Sekizawa et al., 2020). Moreover, they performed various thicknesses of TiO_2 (10, 30, 60, 80 and 120 nm) over the $Pt/TiO_2/Cr_2O_3$ to define photocathode performance, suggesting lower TiO_2 deposition (30 nm) increased photocurrent density and the further TiO_2 coverage blocks desired p-type behaviour of the Cr_2O_3 as a photocathode. Nasir and coworker(Mohd Nasir et al., 2016) obtained Cr_2O_3/CuO:Ni (p-p) photocathode for photoelectrochemical water splitting by chemical vapour deposition (Cr_2O_3) and sol-gel method (CuO:Ni). It indicates that Cr_2O_3/CuO heterojunction (p-p), the photocurrent density of Cr_2O_3 was increased from 0.1 to 1.33 mA cm^{-2} under 1.0 sun in 0.5 M Na_2SO_4 electrolyte.

In this study, we obtained a photostable Cr_2O_3@CuO heterostructure with a new synthesis deposition combination hydrothermal deposition and chronoamperometric deposition, without doping expensive metals. We investigated CuO deposition duration (15, 30 and 45 minutes) impact on photostability and photocatalytic performance over the Cr_2O_3@CuO in the HER process. The photoelectrochemical performance tests of photocathodes indicate that Cr_2O_3 photocurrent density increased 9 times to -1.111 mA cm^{-2} (-0.5 V vs. Ag/AgCl) for chronoamperometric deposition of CuO for 30 minutes (S30) under 100 mW cm^{-2} solar irradiance.

2. EXPERIMENTAL

2.1. Materials

D-glucose, acetone, phosphate buffer (pH 7), lactic acid, ethyl alcohol, KCl, $CuSO_4{\times}5H_2O$, Na_2SO_3 and $Cr(NO_3)_3{\times}5H_2O$ were purchased from Sigma–Aldrich. Fluorine-doped tin oxide (FTO,~8Ω/Sq.) was obtained from Teknoma Company. Furthermore, the applied chemicals were used without a purification process.

2.2. Methods

2.2.1. Electrode Preparation

We performed the synthesis of Cr_2O_3 nanoballs over the FTO substrate (0.8 × 1.25 cm) by the hydrothermal deposition (Faki et al., 2024). The deposition of Cr_2O_3 nanoballs was carried out at the autoclave at 90 °C for 24 hours in a 50 mM $Cr(NO_3)_3{\times}5H_2O$, 50 mM D-glucose and 50 mM KCl deposition bath. The Cr_2O_3 samples were cleaned with distilled water and dried at

DOI: http://dx.doi.org/10.32571/ijct.1863360 E-ISSN: 2602-277X

40°C in an oven under air. Afterward, Cr_2O_3 was calcined in a muffle furnace at 500 °C for 2 hours under an air atmosphere.

CuO was synthesised on Cr_2O_3 nanoballs by electrochemical deposition. It was performed cathodic at -0.25 mA cm^{-2} in 1.0 M lactic acid–0.1 M $CuSO_4 \times 5H_2O$ at 45 °C during various depositions (15, 30 and 45 minutes and the samples are called as S15, S30 and S45, respectively. The deposition bath was arranged to pH 11 by 5.0 M NaOH. The chronoamperometric deposition was conducted by a conventional three-electrode system, including Cr_2O_3, Ag/AgCl (3.0 M KCl), and Pt sheet (2 cm^2) as the working electrode, reference electrode, and counter electrode, respectively. After orange Cr_2O_3@CuO photoelectrodes were washed with distilled water and furnace at 500 °C for 2 hours in an air atmosphere for the conversion of Cu_2O to CuO. Subsequently, black-coloured Cr_2O_3@CuO is obtained at the various deposition durations.

2.2.2. Analysis of Electrode

The morphology of the Cr_2O_3, CuO and Cr_2O_3@CuO heterostructure was analysed using a Scanning Electron Microscope (SEM, FEI Quanta 650). The electrode crystal structure was characterised using X-Ray Diffractometers (XRD, PANalytical Empyrean) within a 2θ° range of 20° to 80°. The light capacity for absorption was evaluated using a UV-Vis spectrometer (Agilent, Cary 7000) within a range of 350 to 900 nm.

2.2.3. Photoelectrochemical Set Up

The photoelectrochemical experiments were performed using a potentiostat/galvanostat (CHI 660D) within a conventional three-electrode configuration, comprising photocathodes (0.80 × 1.25 cm^2), Ag/AgCl (3.0 M KCl) as the reference electrode, and a Pt sheet (2 cm^2) serving as the auxiliary electrode. The electrolyte comprised 0.1 M phosphate buffer and 0.1 M Na_2SO_3. A Xe arc lamp was utilised to achieve a solar power of 100 mW cm^{-2} (Sunlite TM Solar Simulators, M-SLSS, 300 W, light spectrum of 280-1100 nm) with an AM 1.5 filter.

Lineer Sweep voltammetry (LSV) measurements were carried a scan rate of 5 mV s^{-1}, covering a potential value range of 0.0 V to -0.5 V (vs. Ag/AgCl). EIS measurements were conducted with a bias potential at -0.5 V vs. Ag/AgCl with an amplitude of 5 mV in a frequency range from 10^5 to 10^0 Hz under 100 mW cm^{-2} solar light. EIS results of the samples were fitted by ZView software to attain photoelectrochemical parameters at the photoelectrode/electrolyte interface. Mott–Schottky measurements were carried out at an AC amplitude of 5 mV at 500 Hz under dark after the setup of the electrochemical equilibrium for 30 minutes.

3. RESULTS and DISCUSSION

3 .1. Electrode characterization

The Figure 1 displays Tauc plot of photocathodes. The band gap (E_g)value can be determined using a Tauc plot by plotting $(\boldsymbol{\alpha h\nu})^2$ versus $\boldsymbol{h\nu}$. E_g of photocathodes are calculated by following the Tauc equation 1:

$$(\alpha h\nu)^{1/n} = B(h\nu - E_g) \quad (1)$$

In this, α, h, n,ν, and B are the quantity of absorption, the Planck constant, the direct band transition of semiconductor ($n=1/2$), the frequency of light and the experimental constant, respectively. At the binary electrodes, the $(\boldsymbol{\alpha h\nu})^2$ increases with electrochemical deposition duration from 15 to 45 minutes. It can be concluded with the increasing thickness of the CuO layer on the FTO, leading to further light absorption in a binary heterostructure. Cr_2O_3, CuO, S15, S30 and S45 1.90, 1.46, 1.54, 1.54 and 1.53 eV, respectively. It indicates that a decrease in electrochemical deposition duration leads to decreasing of E_g of photocathodes.

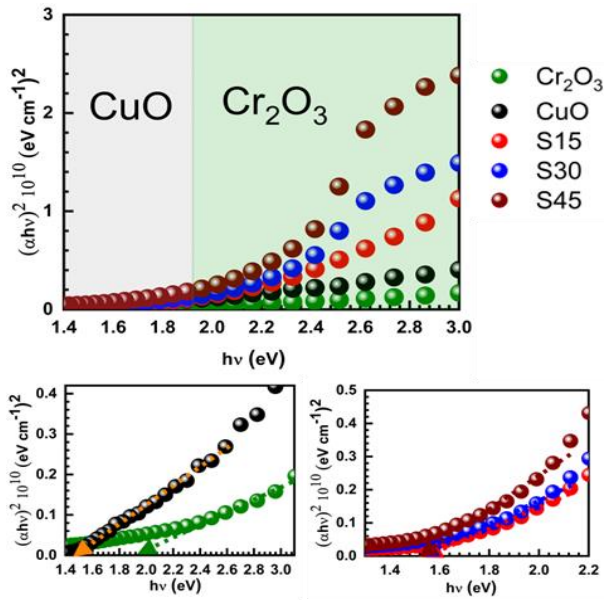


Figure 1. Tauc plot of photocathodes.

SEM images of the electrodes are given in Figure 2. It indicates that the CuO layer grows over the FTO substrate, forming stacked angular layers. On the other hand, Cr_2O_3 crystal growth performs a nanosphere form on the FTO layer, but the size of the Cr_2O_3 nanosphere differs from each other. Additionally, it suggests that nanospheres of similar size and morphology are formed on the surfaces of the S15, S30, and S45 electrodes with the synthesis of CuO at different electrochemical deposition times. Cross-section images were conducted to show the formation of the CuO layer on FTO at different thicknesses over varying deposition durations. A layer of thickness was measured by the ImageJ program.

DOI: http://dx.doi.org/10.32571/ijct.1863360 E-ISSN: 2602-277X

The thickness of CuO:Cr_2O_3 0.668:1.501 µm, 1.201:1.908 µm and 1.618:2.501 µm are calculated for S15, S30 and S45, respectively. It clearly confirms that increasing the electrochemical deposition duration leads to raising the thickness of the CuO layer at the binary electrodes, but it is not affected Cr_2O_3 nanosphere growth process. Furthermore, average particle size of Cr_2O_3, S15, S30 and S45 is measured 902, 766, 887 and 884 nm, respectively. It indicates that Cr_2O_3 nanosphere particle size approximately is not altered with electrochemical CuO deposition duration.

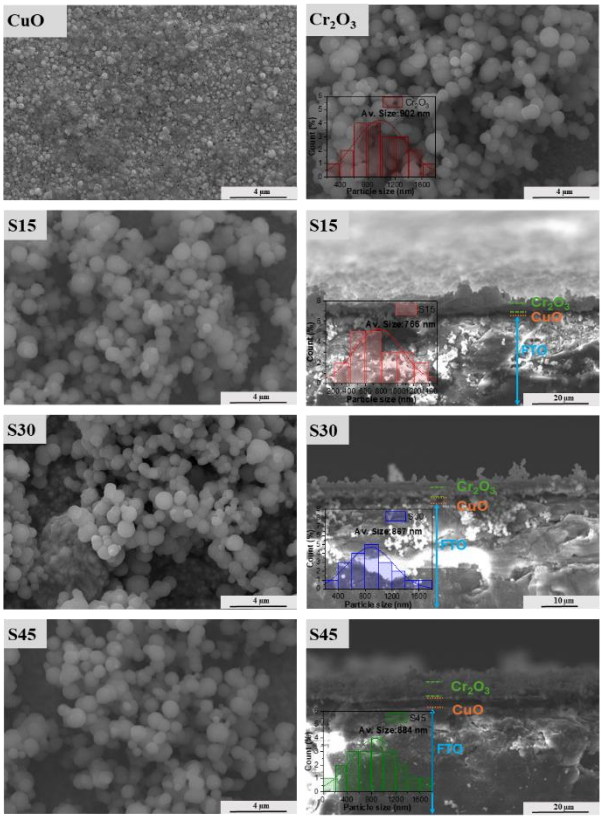


Figure 2. SEM images of photoelectrodes.

Figure 3 depicts the XRD pattern of photocathodes. XRD pattern peaks of CuO at 2θ° values 32.57°, 35.49°, 38.71°, 48.82°, 53.41°, 66.24° and 68.05 correspond to hkl parameters (110), (11$\bar{1}$), (111), (20$\bar{2}$), (020), (31$\bar{1}$) and (220), respectively (JCPDS NO-98-062-8616, ICSD:628616). It demonstrates the main 2θ peaks of 35.49° and 38.71°, suggesting a typical monoclinic crystal structure of CuO. Besides, both primary intensity of peaks enlarges with the increasing electrochemical deposition duration. It could be concluded that the thickness of the CuO layer extends with applied process duration from 15 to 45 minutes. The XRD pattern of Cr_2O_3 exhibits distinct peaks at 2θ angles of 24.44°, 36.45°, and 41.55°, corresponding to the hkl parameters (012), (110), and (006), respectively (JCPDS NO-98-020-2619). It proposes a characteristic rhombohedral structure of Cr_2O_3. However, Cr_2O_3 2θ° peak of 24.44° disappears in the heterostructure electrodes. We suggest that it performs with an applied second calcination process for CuO synthesis. On the other hand, peak intensity of 36.45° is decreased with increasing electrochemical CuO deposition, resulting in a CuO layer predominant over CuO/Cr_2O_3 heterostructure. Consequently, increasing the duration of CuO deposition causes a predominance of CuO, thereby diminishing the electrochemical deposition of the main characteristic of Cr_2O_3 in the binary photocathode.

EIS analysis can determine resistance sources at the photoelectrode/electrolyte interface under applied negative bias voltage and illumination conditions(Lazanas et al., 2023). EIS measurements conducted without applying a bias potential, the electrode resistance provides insight into the non-Faradaic process under steady-state conditions, while the HER occurring at the photocathode under negative bias potential contributes to understanding of the Faradaic process. Therefore, EIS was performed at a bias potential of -0.5 V. Figure 4 depicts the Nyquist (a) and Bode (b) plots of photocathodes exposed to 100 mW cm^{-2} sun irradiation. In the EIS approach, the diameter of the circle corresponds to the magnitude of the resistance value of the electrode. According to the Nyquist plot, Cr_2O_3 performs the highest radius semicircle, but binary heterostructures achieve lower resistance by loading CuO layers. It indicates that the Cr_2O_3/CuO heterostructure interface enables an active HER process with applied bias potential under light. The resistance of binary electrodes changes with S15, S45, and S30 order, indicating that S30 results in the low resistance but rather closed to S45 in the HER process. It can be concluded that both S30 and S45 perform catalytic activity electrode/electrode boundary interface.

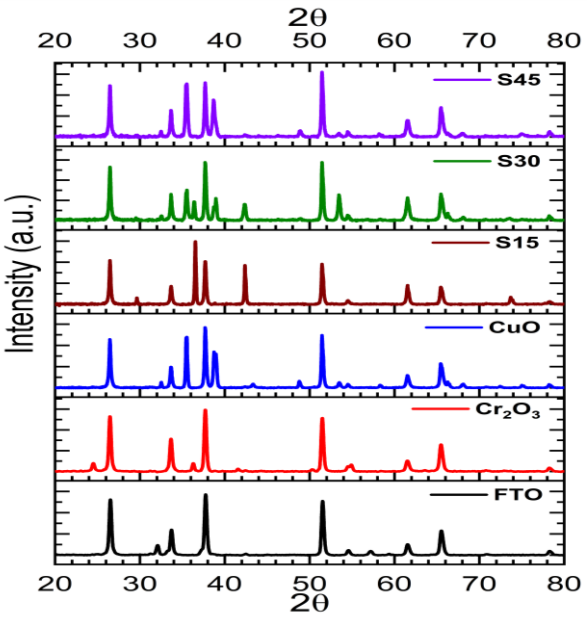


Figure 3. XRD pattern of photocathodes.

DOI: http://dx.doi.org/10.32571/ijct.1863360 E-ISSN: 2602-277X

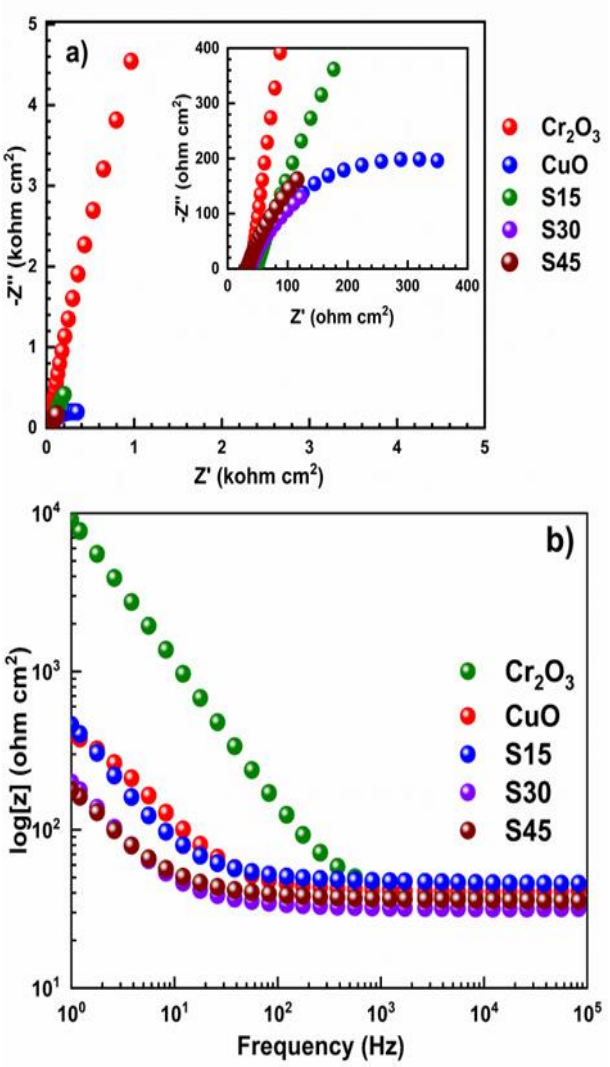


Figure 4. Nyquist and Bode plot of photocathodes in the 0.1 M phosphate buffer and 0.1 M Na_2SO_3 and under 100 mW cm^{-2} solar light irradiation.

In the Bode plot, the beginning point corresponds to the solution resistance (R_s), while the difference between the lowest frequency point and R_s corresponds to the total electrode resistance (R_p). According to Bode plot, S30 performs the lowest R_s value at the highest frequency, S45 shows the least resistance at the lowest frequency, suggesting that charge transfer process clearly occurs over the S45 electrode. It can be assumed that S45 electrode photocatalytic electrode in HER process. The calculated R_p value is given in Table 1, indicating R_p is decreased by electrochemical CuO deposition to Cr_2O_3 photoelectrode, and S30 performs the lowest R_p value compared to all samples. It could be concluded that an appropriate CuO loading layer establishes an electrochemical deposition duration of 30 and 45 minutes and an electron transfer pathway through the energy level of CuO and Cr_2O_3 for the S30 and S45 electrode.

Table 1. R_p value of the photoelectrodes.

Electrode	R_p (Ω cm^2)
Cr_2O_3	9037.8
CuO	359.9
S15	414.4
S30	146.0
S45	163.4

LSV measurement was conducted under solar light by negative scanning from 0.0 to -0.5 V to gain insight into HER performance of photocathodes and is shown in Figure 5. It shows binary heterostructure facilitates enhancement photocurrent-density comparison of pristine Cr_2O_3 and CuO electrodes. In the photoelectrochemical hydrogen production cell, electrons are excited from the valence band (VB) to the CB of Cr_2O_3 and recombination performs from CB of Cr_2O_3 to VB of CuO. The relative recombination in the energy levels can vary depending on the appropriate binary Cr_2O_3 and CuO film thickness. Therefore, the photocurrent density in the binary heterostructure varies, and it can be stated that the optimum film thickness belongs to the S45 electrode. The photocurrent density is measured at -0.5 V, Cr_2O_3, CuO, S15, S30 and S45 -0.024, -0.527, -0.409, -0.532, and -0.911 mA cm^{-2}, respectively. It suggests that the photocurrent density is slightly increased as electrochemical deposition is applied for 45 minutes, resulting in further CuO layer activated under solar light (Mahmood et al., 2017; Siavash Moakhar et al., 2021). The LSV results corroborate the XRD pattern, indicating that the peak intensity at 36.45° diminishes with the increasing electrochemical deposition of CuO, leading to a predominance of the CuO layer over the CuO/Cr_2O_3 heterostructure.

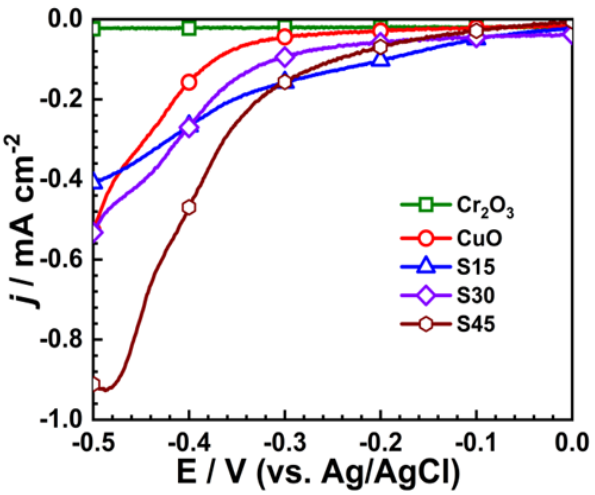


Figure 5. LSV of photocathodes in the 0.1 M phosphate buffer and 0.1 M Na_2SO_3 and under 100 mW cm^{-2} solar light irradiation.

DOI: http://dx.doi.org/10.32571/ijct.1863360 E-ISSN: 2602-277X

The Mott-Schottky measurement can be used to determine the type of semiconductor in photoelectrodes and the flat band (E_{fb})(Cardon et al., 1978a; Lasia, 2014). The Mott-Schottky measurement was carried out in the dark at 1.0-0.0 V (vs. Ag/AgCl) and is shown in Figure 6. In the photoelectrochemical cell, p-type semiconductor is preferred as a photocathode. A negative slope confirms the p-type nature of photoelectrodes. Consequently, we propose that the obtained electrodes possess the potential to operate as photocathodes. The E_{fb} of the samples can be determined by applying the Mott-Schottky measurement with the following equation 2.

$$\frac{1}{C^2} = \frac{2}{q\,\varepsilon_s\,\varepsilon_0 N_D}\left[E - E_{fb} - \frac{k_B T}{q}\right] \qquad 2$$

According to these equations, C is the charge capacitance of of the sample, q is the charge of an electron, ε_0 is the permittivity of vacuum (8.854 pF/m), ε_s is the dielectric constant of the samples (65) , T is the experimental conditions, k_B is the Boltzmann constant, and E is the applied a bias potential.

Table 2. E_{fb} values of photoelectrodes.

Electrode	E_{fb} (V vs. Ag/AgCl)
S15	0.749
S30	0.997
S45	0.966

The E_{fb} values calculated using the Mott-Schottky measurement of photoelectrons are shown in Table 2. According to Mott-Schottky approach, an p-type semiconductor material to shift towards a negative potential to exhibit more photocatalytic behaviour in the photoelectrochemical cells (Albery et al., 1996; Cardon et al., 1978b). A variety of electrochemical CuO deposition duration, leading to an alteration in the Fermi energy level of the electrodes within the electrolyte, thereby caused the E_{fb} values to shift to a more positive potential. It suggests that S30 sample performs more positive potential, enable further electron transfer among the energy levels of Cr_2O_3 and CuO to conversion H^+ ion to H_2 molecule with solar irradiation. Therefore, it can be conculcated that S30 and S45 photocathode achieves further H_2 production in the photoelectrochemical cell.

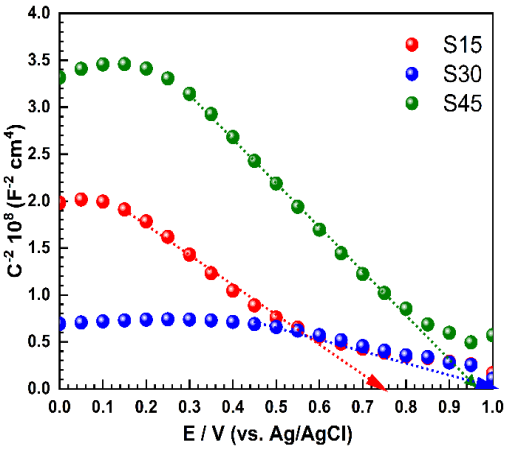


Figure 6. Mott-Schottky plot of photocathodes in the 0.1 M phosphate buffer and 0.1 M Na_2SO_3 and under dark condition.

4.CONCLUSION

We performed a binary Cr_2O_3@CuO heterostructure with a new synthesis deposition combination hydrothermal deposition and chronoamperometric deposition. SEM images indicate that CuO layer grows stacked angular layers, and Cr_2O_3 crystal growth performs a nanosphere form on the FTO layer. EIS results demonstrate the resistance of binary electrodes changes with S15, S45, and S30 order, indicating that S30 results in the lowest resistance in the HER process. According to LSV, the photocurrent density is measured at -0.5 V Cr_2O_3, CuO, S15, S30 and S45 -0.024, -0.527, -0.409, -0.532, and -0.911 mA cm^{-2}, respectively. Mott-Schotkky measurement suggests that S45 sample performs more negative potential, enabling further electron transfer among the energy levels of Cr_2O_3 and CuO to HER process under solar irradiation.

Acknowledgements

The authors are thankful to Çukurova University, Science and Letters Faculty, Chemistry Department, Physical Chemistry Research Laboratory and Tarsus University for laboratory studies.

Conflict of Interest

The authors declare that they have no known competing financial interests or personal relationships that could have appeared to influence the work reported in this paper.

DOI: http://dx.doi.org/10.32571/ijct.1863360 E-ISSN: 2602-277X

Ethical Statement

The authors declare that they have no known competing financial interests or personal relationships that could have appeared to influence the work reported in this paper.

REFERENCES

Albery, W. J., O'Shea, G. J., & Smith, A. L. (1996). Interpretation and use of Mott–Schottky plots at the semiconductor/electrolyte interface. *Journal of the Chemical Society, Faraday Transactions*, *92*(20), 4083–4085.

Cardon, F., & Gomes, W. P. (1978a). On the determination of the flat-band potential of a semiconductor in contact with a metal or an electrolyte from the Mott-Schottky plot. *Journal of Physics D: Applied Physics*, *11*(4), L63–L63.

Cardon, F., & Gomes, W. P. (1978b). On the determination of the flat-band potential of a semiconductor in contact with a metal or an electrolyte from the Mott-Schottky plot. *Journal of Physics D: Applied Physics*, *11*(4), L63.

Chiu, Y.-H., Lai, T.-H., Kuo, M.-Y., Hsieh, P.-Y., & Hsu, Y.-J. (2019). Photoelectrochemical cells for solar hydrogen production: Challenges and opportunities. *APL Materials*, *7*(8), 080901. https://doi.org/10.1063/1.5109785

da Silva Veras, T., Mozer, T. S., da Costa Rubim Messeder dos Santos, D., & da Silva César, A. (2017). Hydrogen: Trends, production and characterization of the main process worldwide. *International Journal of Hydrogen Energy*, *42*(4), 2018–2033. https://doi.org/10.1016/j.ijhydene.2016.08.219

Faki, E., Tezcan, F., & Kardas, G. (2024). Investigation of photocatalytic performance of p-type Cr_2O_3 photocathode for hydrogen evolution reaction. *Niğde Ömer Halisdemir University Journal of Engineering Sciences*, *13*(3).

Kayan, D. B. (2023). Hydrogen production via water electrolysis on an active electrocatalyst rGONi nanocomposite. *International Journal of Chemistry and Technology*, *7*(1), 1–5.

Khelifa, A. B., Soum-Glaude, A., Khamlich, S., Glénat, H., Balghouthi, M., Guizani, A. A., Maaza, M., & Dimassi, W. (2019). Optical simulation, characterization and thermal stability of Cr_2O_3/Cr/Cr_2O_3 multilayer solar selective absorber coatings. *Journal of Alloys and Compounds*, *783*, 533–544. https://doi.org/10.1016/j.jallcom.2018.12.286

Lasia, A. (2014). Semiconductors and Mott-Schottky plots. In *Electrochemical impedance spectroscopy and its applications* (pp. 143–174). Springer. https://doi.org/10.1007/978-1-4614-8933-7_10

Lazanas, A. Ch., & Prodromidis, M. I. (2023). Electrochemical impedance spectroscopy—A tutorial. *ACS Measurement Science Au*, *3*(3), 162–193. https://doi.org/10.1021/acsmeasuresciau.2c00070

Liu, J., Chen, T., & Hu, B. (2023). Consumer acceptance under hydrogen energy promotion policy: Evidence from Yangtze River Delta. *International Journal of Hydrogen Energy*, *48*(30), 11299–11312. https://doi.org/10.1016/j.ijhydene.2022.07.081

Mahmood, A., Tezcan, F., & Kardaş, G. (2017). Photoelectrochemical characteristics of CuO films with different electrodeposition time. *International Journal of Hydrogen Energy*, *42*(36), 23032–23041. https://doi.org/10.1016/j.ijhydene.2017.06.003

Mahmoud, H. R. (2014). Highly dispersed Cr_2O_3–ZrO_2 binary oxide nanomaterials as novel catalysts for ethanol conversion. *Journal of Molecular Catalysis A: Chemical*, *392*, 216–222. https://doi.org/10.1016/j.molcata.2014.05.021

Mansoor, M. A., Munawar, K., Naeem, R., Sarih, N. M., Asghar, M. A., Haider, A., Zubir, M. N. M., & Zaharinie, T. (2023). Aerosol-assisted facile fabrication of bimetallic Cr_2O_3–Mn_2O_3 thin films for photoelectrochemical water splitting. *New Journal of Chemistry*, *47*(17), 8347–8354. https://doi.org/10.1039/D2NJ06274G

Mohd Nasir, S. N. F., Yahya, M. K. N., Mohamad Sapian, N. W., Ahmad Ludin, N., Ibrahim, M. A., Sopian, K., & Mat Teridi, M. A. (2016). Heterojunction Cr_2O_3/CuO photocathodes for enhanced photoelectrochemical performance. *RSC Advances*, *6*(62), 57510–57517. https://doi.org/10.1039/C6RA03904A

Moakhar, R. S., Hosseini-Hosseinabad, S. M., Masudy-Panah, S., Seza, A., Jalali, M., Fallah-Arani, H., Dabir, F., Gholipour, S., Abdi, Y., Bagheri-Hariri, M., Riahi-Noori, N., Lim, Y. F., Hagfeldt, A., & Saliba, M. (2021). Photoelectrochemical water-splitting using CuO-based electrodes for hydrogen production: A review. *Advanced Materials*, *33*(33), 2007285. https://doi.org/10.1002/adma.202007285

Sekizawa, K., Oh-Ishi, K., & Morikawa, T. (2020). Photoelectrochemical water-splitting over a surface-modified p-type Cr_2O_3 photocathode. *Dalton Transactions*, *49*(3), 659–666. https://doi.org/10.1039/C9DT04296B

Tezcan, F., & Demir, D. (2023). 3D TiO_2 modified with reduced graphene embed into polyvinyl alcohol: photoanode electrode for oxygen evolution reaction. *International Journal of Chemistry and Technology*, *7*(2), 189–196.

Tezcan, F., Kahya Düdükcü, M., & Kardaş, G. (2022). Photocorrosion protection of $BiVO_4$ electrode by α-Cr_2O_3 core–shell for photoelectrochemical hydrogen production. *Journal of Electroanalytical Chemistry*, *920*, 116595. https://doi.org/10.1016/j.jelechem.2022.116595

Zelekew, O. A., Fufa, P. A., Sabir, F. K., & Duma, A. D. (2021). Water hyacinth plant extract mediated green synthesis of Cr_2O_3/ZnO composite photocatalyst for the degradation of organic dye. *Heliyon*, *7*(7), e07652. https://doi.org/10.1016/j.heliyon.2021.e07652